

Free energy landscape from path-sampling: application to the structural transition in LJ₃₈

G. Adjanor¹, M. Athènes^{1,a}, and F. Calvo²

¹ Service de Recherches de Métallurgie Physique, Commissariat à l'Énergie Atomique/Saclay, 91191 Gif-sur-Yvette, France

² Laboratoire de Chimie et Physique Quantiques, IRSAMC, Université Paul Sabatier, 118 route de Narbonne, 31062 Toulouse Cedex, France

Received 31 May 2006 / Received in final form 27 July 2006

Published online 22 September 2006 – © EDP Sciences, Società Italiana di Fisica, Springer-Verlag 2006

Abstract. We introduce a path-sampling scheme that allows equilibrium state-ensemble averages to be computed by means of a biased distribution of non-equilibrium paths. This non-equilibrium method is applied to the case of the 38-atom Lennard-Jones atomic cluster, which has a double-funnel energy landscape. We calculate the free energy profile along the Q_4 bond orientational order parameter. At high or moderate temperature the results obtained using the non-equilibrium approach are consistent with those obtained using conventional equilibrium methods, including parallel tempering and Wang-Landau Monte Carlo simulations. At lower temperatures, the non-equilibrium approach becomes more efficient in exploring the relevant inherent structures. In particular, the free energy agrees with the predictions of the harmonic superposition approximation.

PACS. 07.05.Tp Computer modeling and simulation – 36.40.Ei Phase transitions in clusters – 64.70.Pf Glass transitions – 82.60.Lf Thermodynamics of solutions

1 Introduction

The calculation of free energies remains a challenge in computer simulation for systems with complex energy landscapes, having numerous basins of attraction separated by large energy barriers. A drastic slowing down of numerical convergence, often referred to as broken ergodicity, is observed when the system gets trapped in a few metastable minima at sufficiently low temperature. As a consequence of broken ergodicity, free energies or even standard thermodynamic averages cannot be estimated directly. Dedicated algorithms have been designed to determine free energies relative to a known reference. Following Torrie and Valleau [1], regions of phase space with a naturally low visiting probability, such as saddles or transition states, can be sampled using an auxiliary non-physical potential added to the Hamiltonian. This so-called umbrella potential lowers the energy barriers once a suitable order parameter is available. This relatively old idea is still the subject of technical improvements. For instance, implementations using biasing potentials [2–5], possibly constructed systematically using the smarter and systematic Wang-Landau scheme [6, 7], have been proposed.

Other efficient algorithms have been inspired by the thermodynamic perturbation and integration methods, which are very similar to the way free energy differences

are obtained experimentally. Constraint techniques in the framework of the so-called blue-moon ensemble [8] integrate the free energy derivative with respect to an adequate reaction coordinate. In the slow (adiabatic [9]) and fast (non-equilibrium [10]) switching methods, paths are generated in order to connect one reference system to the target system, and the free energy difference between them is obtained by averaging over the work along one very long trajectory or many short trajectories, respectively. Such path sampling methods have a strong advantage over conventional algorithms based on configurations alone, because the work carries more information than the irregular set of corresponding phase space points. In addition, the entire properties can be continuously obtained along the path. Sampling paths instead of configurations is also a key ingredient in recent numerical methods such as transition path sampling [11] or discrete path sampling [12] in reaction dynamics, and is ubiquitous in quantum statistics [13, 14].

One of us previously proposed a path sampling scheme to compute thermodynamic properties at equilibrium, in which the paths are generated from a generalized ensemble [15]. In the present paper we apply this method to the 38-atom Lennard-Jones (LJ) cluster, denoted as LJ₃₈ hereafter. This system is particularly troublesome to study numerically because its potential energy landscape has two main funnels [16]. At low temperature, a structural

^a e-mail: Manuel.Athenes@cea.fr

transition takes place between the lowest energy (truncated octahedral, or cubic) funnel and the higher energy (icosahedral) funnel, which also has a higher entropy. The large energy barriers separating the two funnels are responsible for broken ergodicity in conventional simulations. The rates for crossing this barrier, as estimated from the master equation approach [17] or, more recently, from the discrete path sampling method [18], are extremely low, the time scales being more than 10 orders of magnitude longer than the vibrational period.

Using the bond orientational order parameter Q_4 introduced by Steinhardt et al. [19], Doye and coworkers [16] performed multicanonical-type umbrella sampling simulations and estimated the Landau free energy barriers as a function of Q_4 , thus mapping the structural transition. Unfortunately, these authors were able to get converged data only at temperatures above the melting point, but failed to sample properly the configuration space in the vicinity of the transition temperature itself. Successful parallel tempering [20] simulations and Wang-Landau simulations [6] have been carried out for the heat capacity of this cluster (see Refs. [21] and [22], respectively), but no Landau free energies have been reported, to our knowledge.

The LJ₃₈ cluster thus appears as a good candidate for testing the set of methods described in reference [15], especially the possible benefits from a generalized ensemble strategy. As will be shown below, path sampling gives accurate free energy profiles as a function of the Q_4 order parameter and in a broader temperature range, down to temperatures where other methods fail.

The article is organized as follows. The standard umbrella sampling method is briefly recalled in Section 2 and, using tools developed in reference [15], the path sampling approach is extended in Section 2.2 so as to incorporate the auxiliary umbrella potential. The configurational-bias scheme recently proposed by Wu and Kofke [23] to construct the paths is described in Section 3. Our application to LJ₃₈, with comparison to available data from the literature and alternative estimates from dedicated simulations, is presented in Section 4. We summarize and give some final remarks in Section 5. Some technical issues about the Langevin-Metropolis algorithm used to propagate the path dynamics are detailed in the Appendix.

2 Computational method

The coordinates of the many-body system are, in vector notation,

$$\mathcal{S} = (\mathbf{r}, \mathbf{p}) \quad (1)$$

where \mathbf{r} and \mathbf{p} correspond to the set of positions and momenta, respectively. Let $\mathcal{E}(\mathbf{r})$ be the inter-particle potential energy. The Hamiltonian is thus defined as

$$\mathcal{H}(\mathbf{r}, \mathbf{p}) = \frac{\mathbf{p}^2}{2m} + \mathcal{E}(\mathbf{r}) \quad (2)$$

where $\mathbf{p}^2/2m$ is the classical kinetic energy.

The standard ensemble-average in the canonical ensemble at constant inverse temperature β_λ is

$$\langle \mathcal{A} \rangle_\lambda = \frac{\int \mathcal{A}(\mathbf{r}) \exp[-\beta_\lambda \mathcal{H}(\mathbf{r}, \mathbf{p})] d\mathcal{S}}{\int \exp[-\beta_\lambda \mathcal{H}(\mathbf{r}, \mathbf{p})] d\mathcal{S}}. \quad (3)$$

In systems exhibiting broken ergodicity, it is not possible to estimate the thermodynamic properties from direct sampling of equation (3) because the system gets trapped in a restricted phase space volume. Umbrella sampling alleviates this problem for systems with smooth energy landscapes: an auxiliary potential is added to the system Hamiltonian in order to facilitate the crossing of barriers between the important basins of attraction. A suitable order parameter Q is introduced in order to discriminate the various basins of attraction. A multicanonical procedure is then implemented to construct iteratively the adequate auxiliary potential leading to a flat sampling along the order parameter.

In practice, the multicanonical procedure fails to construct the adequate auxiliary potential at low temperatures when the system exhibits a rugged free energy landscape. The idea of the present study is to carry out the umbrella-sampling simulation in a path-ensemble. The non-equilibrium paths of the path-ensemble will connect a state-ensemble at a high temperature T_0 , for which the auxiliary potential can be easily constructed, to a state-ensemble at a low temperature for which building the auxiliary potential would be much more difficult.

Since paths will be initiated from states generated by means of a multicanonical-type umbrella sampling simulation, this method is now briefly recalled.

2.1 Umbrella sampling

Let $\phi(\mathbf{r})$ be an auxiliary potential aimed at sampling specific regions of the energy surface. A parametrized Hamiltonian \mathcal{H}_λ is introduced such that

$$\mathcal{H}_\lambda(\mathbf{r}, \mathbf{p}) = \frac{\mathbf{p}^2}{2m} + [\beta_\lambda \mathcal{E}(\mathbf{r}) + \phi(\mathbf{r})] / \beta \quad (4)$$

where β is a constant having the dimension of an inverse temperature. The associated unnormalized Boltzmann weight of state \mathcal{S} corresponding to this Hamiltonian,

$$\mathcal{N}_\lambda(\mathcal{S}) = \exp[-\beta \mathcal{H}_\lambda(\mathbf{r}, \mathbf{p})], \quad (5)$$

defines a non-physical umbrella ensemble, noted \mathcal{Z}_λ , from which ensemble-averages can be obtained as

$$\langle \mathcal{A} \rangle_\lambda \equiv \langle \mathcal{A} |_\lambda \rangle = \frac{\int \mathcal{A}(\mathbf{r}) \mathcal{N}_\lambda(\mathcal{S}) \exp \phi(\mathbf{r}) d\mathcal{S}}{\int \mathcal{N}_\lambda(\mathcal{S}) \exp \phi(\mathbf{r}) d\mathcal{S}}. \quad (6)$$

The notation for the average has been changed from $\langle \mathcal{A} \rangle_\lambda$ to $\langle \mathcal{A} |_\lambda \rangle$ to clearly indicate that the reference distribution that is sampled now differs from the original canonical distribution at temperature β_λ and Hamiltonian \mathcal{H} . Hence, if a Markov chain is constructed with the states distributed according to the \mathcal{N}_λ -statistics (using for instance

the Metropolis algorithm), then the canonical average can be recovered from the standard reweighting formula

$$\langle \mathcal{A} \rangle_\lambda \equiv \langle \mathcal{A} |_\lambda \rangle = \frac{\sum_{\mathbf{r}_q} \mathcal{A}(\mathbf{r}_q) \exp \phi(\mathbf{r}_q)}{\sum_{\mathbf{r}_q} \exp \phi(\mathbf{r}_q)}, \quad (7)$$

where the summation runs over states of the Markov chain propagated with \mathcal{H}_λ .

2.2 Umbrella path-sampling

As aforementioned, generating the multicanonical weight for an optimal umbrella sampling procedure works best at relatively high temperatures. At moderate or low temperatures, achieving a flat sampling over a wide range of the order parameter becomes computationally hard. The solution to the problem that is presented here consists in estimating the canonical average by means of a *chain of non-equilibrium states*. The non-equilibrium states are generated by a series of stochastic dynamical processes initiated from states homogeneously distributed along the order parameter at the highest temperature T_0 . Moreover the temperature is artificially decreased during each trajectory. This series of stochastic quenches thus corresponds to a distribution of non-equilibrium paths.

In order to deal with such path distributions, we use the path-ensemble formalism introduced in reference [15]. Keeping the same path-ensemble notations, $\hat{\mathcal{Z}}_\lambda$ stands for the path-ensemble whose statistical averages formally coincide with the averages in the state ensemble \mathcal{Z}_λ . The set of all possible paths \mathcal{P}_i^f defines the path phase-space Ω and $\hat{\mathcal{K}}_\lambda(\mathcal{P}_i^f)$ stands for the path statistical weight in $\hat{\mathcal{Z}}_\lambda$, equivalent of an unnormalized Boltzmann weight.

A path \mathcal{P}_i^f consists of a set of K states constructed by means of a stochastic procedure detailed below. In the present study, the paths are generated forward in time starting from an initial state denoted as \mathcal{S}_i . This state itself is generated according to the \mathcal{Z}_{λ_0} statistics. The path goes through the set of states \mathcal{S}_k belonging to \mathcal{Z}_λ with $\lambda = \lambda_{mn}$, $0 \leq m \leq M$ and $0 \leq n \leq N$, and ends in the state \mathcal{S}_f belonging to the $\mathcal{Z}_{\lambda_{MN}}$ ensemble where M and N are two integers. A path is a juxtaposition of segments, called branches, each one containing N states. They are constructed using the configurational-bias scheme detailed in the following subsection.

The conditional probabilities associated to the stochastic process are a key ingredient of path-sampling and will be considered first, momentarily leaving aside their explicit analytical form. Any path \mathcal{P}_i^f can be decomposed into two partial paths $\mathcal{P}^{i \rightarrow k}$ and $\mathcal{P}^{k \rightarrow f}$, which connect \mathcal{S}_i to \mathcal{S}_k and \mathcal{S}_k to \mathcal{S}_f , respectively. The conditional probabilities to start from \mathcal{S}^k and to generate the path segment $\mathcal{P}^{i \rightarrow k}$ backward in time or the path segment $\mathcal{P}^{k \rightarrow f}$ forward in time are denoted as $P_{cond}^-(\mathcal{P}^{i \rightarrow k})$ and $P_{cond}^+(\mathcal{P}^{k \rightarrow f})$, respectively. The statistical weight of a path \mathcal{P}_i^f considered with respect to the $\hat{\mathcal{Z}}_\lambda$ ensemble is now

$$\hat{\mathcal{K}}_\lambda(\mathcal{P}_i^f) = P_{cond}^-(\mathcal{P}^{i \rightarrow k}) \mathcal{N}_\lambda(\mathcal{S}^k) P_{cond}^+(\mathcal{P}^{k \rightarrow f}). \quad (8)$$

The ensemble average of equation (7) can now be transposed into the path ensemble

$$\langle \mathcal{A} |_\lambda \rangle = \frac{\int \mathcal{A}(\mathbf{r}_k) \hat{\mathcal{K}}_\lambda(\mathcal{P}_i^f) \exp \phi(\mathbf{r}_k) d\mathcal{P}_i^f}{\int \hat{\mathcal{K}}_\lambda(\mathcal{P}_i^f) \exp \phi(\mathbf{r}_k) d\mathcal{P}_i^f}, \quad (9)$$

where \mathbf{r}_k are the positions of \mathcal{S}_k . The equivalence between equations (6) and (9) results from the normalization property of the forward and backward conditional probabilities starting from a same given state \mathcal{S}_k :

$$\int_{\Omega_\lambda(\mathcal{S}_k)} d\mathcal{P}_i^f P_{cond}^-(\mathcal{P}^{i \rightarrow k}) P_{cond}^+(\mathcal{P}^{k \rightarrow f}) = 1, \quad (10)$$

where $\Omega_\lambda(\mathcal{S}_k)$ stands for the phase-space volume of all paths that contain a given state $\mathcal{S}_k \in \mathcal{Z}_\lambda$.

In practice, a Markov chain of paths distributed with the $\hat{\mathcal{Z}}_{\lambda_0}$ statistics is constructed. Since λ_0 corresponds to the highest temperature ($T_0 = (k_B \beta \lambda_0)^{-1}$), the entire path \mathcal{P}_i^f is generated forward in time, which in particular implies that the path segments $\mathcal{P}^{i \rightarrow k}$ are generated forward and not backward. These path segments occur with the conditional probability $P_{cond}^+(\mathcal{P}^{i \rightarrow k})$, and they contribute with probability $P_{cond}^-(\mathcal{P}^{i \rightarrow k})$ to the path-average, as can be inferred from equations (8) and (9). Similarly, paths are initiated from states \mathcal{S}_i , which are themselves distributed according to the \mathcal{N}_{λ_0} -statistics; the contribution to the average is the statistical weight $\mathcal{N}_\lambda(\mathcal{S}_k)$. As a consequence, the correcting factors

$$\frac{\mathcal{N}_\lambda(\mathcal{S}_k) P_{cond}^-(\mathcal{P}^{i \rightarrow k})}{\mathcal{N}_{\lambda_0}(\mathcal{S}_i) P_{cond}^+(\mathcal{P}^{i \rightarrow k})} = \frac{\hat{\mathcal{K}}_\lambda(\mathcal{P}_i^f)}{\hat{\mathcal{K}}_{\lambda_0}(\mathcal{P}_i^f)} \quad (11)$$

have to be introduced to reweight the contribution of the paths into any path-ensemble estimate in equation (9). In order to simplify the notations, we define a new quantity, the effective work $\widetilde{\mathcal{W}}^{i \rightarrow k}$, as the logarithm of the probability flux ratio:

$$\exp \left[-\beta \widetilde{\mathcal{W}}^{i \rightarrow k} \right] = \frac{\hat{\mathcal{K}}_\lambda(\mathcal{P}_i^f)}{\hat{\mathcal{K}}_{\lambda_0}(\mathcal{P}_i^f)}. \quad (12)$$

The formal path-average of equation (9) can be estimated by means of the following Monte Carlo average

$$\langle \mathcal{A} |_\lambda \rangle = \frac{\sum_q \mathcal{A}(\mathbf{r}_{kq}) \exp \left[-\beta \widetilde{\mathcal{W}}_q^{i \rightarrow k} + \phi(\mathbf{r}_{kq}) \right]}{\sum_q \exp \left[-\beta \widetilde{\mathcal{W}}_q^{i \rightarrow k} + \phi(\mathbf{r}_{kq}) \right]}, \quad (13)$$

where the \mathbf{r}_{kq} are the positions of state $\mathcal{S}_{kq} \in \mathcal{Z}_\lambda$ for the q th path \mathcal{P}_{iq}^f of the Markov chain. The correcting bias associated to the non-Boltzmann path-average includes the umbrella potential, as in the state-ensemble average in equation (7), and also an effective work related to the path-ensemble.

The Monte Carlo average of equation (13) applies to paths that are generated forward in time by means of any suitable stochastic procedure. However it must be manipulated with caution due to possible problems of numerical convergence. Such problems appear when trajectories

are generated by switching λ too fast, which leads to insufficient overlap between the states along the paths and the target equilibrium state distribution [24]. Recently, Wu and Kofke [23] introduced various Rosenbluth-biased path procedures aimed at favouring trajectories with low-work values, therefore increasing the overlap between the non-equilibrium state distribution and the targeted equilibrium distribution. In the present study we have implemented one of these procedures, namely the configurational-bias scheme [25] that is now described.

3 Configurational-bias scheme

Historically the configurational-bias (CB) scheme [26] was introduced to generate polymer configurations by growing the polymer chain monomer after monomer. At each step, the CB scheme first generates a set of J positions where to insert the current monomer, from which one particular position is selected according to the Rosenbluth rule. This rule favours energetically low polymer conformations. Following Wu and Kofke [23], the configurational-bias scheme is applied to paths rather than real polymers by substituting the branches to the monomers. The ramified nature of the CB algorithm is thus kept in the present path sampling method.

Let $A = \{\lambda_0, \dots, \lambda_{MN}\}$ denote the set of $(MN + 1)$ increasing values of the λ parameter. A path runs through the generalized ensemble $\mathcal{Z} = \bigcup_{\lambda \in A} \mathcal{Z}_\lambda$ and has the ramified structure depicted in Figure 2. This path consists of M stages of J parallel branches. Hence, there are $K = 1 + MNJ$ states in a path. The j th branch of the m th stage, denoted as $B(m, j)$, is generated forward in time by integrating the Langevin-Metropolis algorithm detailed in the Appendix while gradually increasing the parameter λ from $\lambda_{(m-1)N}$ to λ_{mN} in N iterations. The forward and backward conditional probabilities are noted $P_{gen}^+(m, j)$ and $P_{gen}^-(m, j)$, respectively. All branches $B(m, j)$, $1 \leq j \leq J$, are grown from the same initial state $\mathcal{S}_{N(m-1)}^{j_{m-1}}$ corresponding to the final state of the branch $B(m-1, j_{m-1})$ selected previously. This branch is called the trunk and the other branches $B(m, j \neq j_m)$ are called ‘‘dead branches.’’ Denoting \mathcal{S}_{Nm}^j the final state of branch $B(m, j)$, the probability $P_{sel}^+(m, j_m)$ to select $B(m, j_m)$ as the trunk is given by a configurational-bias rule [26]

$$P_{sel}^+(m, j_m) = \frac{\mathcal{N}_{\lambda_{Nm}}(\mathcal{S}_{Nm}^{j_m}) P_{gen}^-(m, j_m) / P_{gen}^+(m, j_m)}{\sum_{j=1}^J \mathcal{N}_{\lambda_{Nm}}(\mathcal{S}_{Nm}^j) P_{gen}^-(m, j) / P_{gen}^+(m, j)},$$

in which the generating probabilities have been included. Note that in the case of sampling polymer configurations the generating probabilities to insert a monomer are always chosen to be symmetric [$P_{gen}^+(m, j) = P_{gen}^-(m, j)$], hence the original Rosenbluth rule omits these terms. If the ramified path is grown backward in time, the position of the trunk among the J branches must be chosen randomly, which implies

$$P_{sel}^-(m, j_m) = 1/J. \quad (14)$$

The conditional probability to generate the ramified path forward (+) or backward (−) in time is

$$P_{cond}^\pm(\mathcal{P}_i^j) = \prod_{m=1}^M \left\{ \left[\prod_{\substack{j=1 \\ j \neq j_m}}^J P_{gen}^+(m, j) \right] \times P_{gen}^\pm(m, j_m) P_{sel}^\pm(m, j_m) \right\} \quad (15)$$

where the dead branches $B(m, j \neq j_m)$ are always generated forward even when the ramified path is generated backward. The generating probabilities of the dead branches $\prod_{\substack{j=1 \\ j \neq j_m}}^J P_{gen}^+(m, j)$ contribute both in the forward and backward probability fluxes. Therefore the exponential of the effective work only contains the generating and selecting probabilities of the branches $B(m, j \neq j_m)$, which belong to the trunk:

$$\begin{aligned} \exp[-\beta \widetilde{\mathcal{W}}^{i \rightarrow f}] &= \frac{\mathcal{N}_{\lambda_{NM}}(\mathcal{S}_f) P_{cond}^-(\mathcal{P}_i^f)}{\mathcal{N}_{\lambda_0}(\mathcal{S}_i) P_{cond}^+(\mathcal{P}_i^f)} \\ &= \prod_{m=1}^M \left[\frac{\mathcal{N}_{\lambda_{Nm}}(\mathcal{S}_{Nm}^{j_m})}{\mathcal{N}_{\lambda_{N(m-1)}}(\mathcal{S}_{N(m-1)}^{j_{m-1}})} \frac{P_{gen}^-(m, j_m)}{P_{gen}^+(m, j_m)} \right. \\ &\quad \left. \times \frac{J^{-1}}{P_{sel}^+(m, j_m)} \right], \quad (16) \end{aligned}$$

with $\mathcal{S}_0^{j_0} = \mathcal{S}_i$ and $\mathcal{S}_{NM}^{j_M} = \mathcal{S}_f$.

In order to cast the last equality into a computationally tractable form, the ratios of probability fluxes are first expressed as a function of the corresponding work introduced into the system from the outside world (see the Appendix):

$$\frac{\mathcal{N}_{\lambda_{Nm}}(\mathcal{S}_{Nm}^{j_m})}{\mathcal{N}_{\lambda_{N(m-1)}}(\mathcal{S}_{N(m-1)}^{j_{m-1}})} \frac{P_{gen}^-(m, j)}{P_{gen}^+(m, j)} = \exp[-\beta \mathcal{W}(m, j)] \quad (17)$$

Similarly, the configurational-bias selecting rule is reformulated as a function of the works $\mathcal{W}(m, j)$ and $\mathcal{W}(m, j_m)$:

$$P_{sel}^+(m, j_m) = \frac{\exp[-\beta \mathcal{W}(m, j_m)]}{\sum_{j=1}^J \exp[-\beta \mathcal{W}(m, j)]}. \quad (18)$$

Equation (18) precisely corresponds to the form proposed by Wu and Kofke [23]. By substituting equations (17) and (18) into equation (16) the exponential of the effective work is related to the Rosenbluth factor as:

$$\exp[-\beta \widetilde{\mathcal{W}}^{i \rightarrow f}] = \frac{1}{J^M} \prod_{m=1}^M \left[\sum_{j=1}^J \exp[-\beta \mathcal{W}(m, j)] \right]. \quad (19)$$

The configurational-bias scheme favours the construction of paths with low work values $\mathcal{W}(m, j_m)$ ($1 \leq m \leq M$). Moreover, since the exponential of these low work values

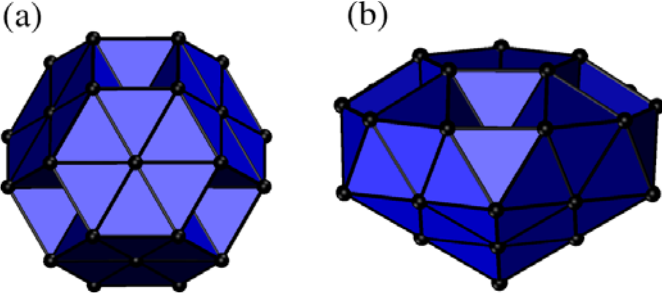


Fig. 1. The two lowest energy structures of the 38-atom cluster: (a) truncated octahedron with energy $E_0 = -173.9284$ and (b) incomplete icosahedron, $E_1 = -173.2524$.

dominates in the Rosenbluth factor, the average dissipated work is smaller and the effective-work distribution is narrower, as can be inferred from the non-equilibrium work and the fluctuation theorem [24, 27–29]. In addition, the overlap between the two histograms of the work that can be constructed by generating the paths either forward or backward is larger. Consequently, numerical convergence of the path-ensemble averages is faster [24].

In the description that has been followed here, the ramifications contain all the statistical biases. All branches, whether they belong to the trunk or not, can be identically taken into account in the path-ensemble average of equation (13). If \mathcal{S}_k is the final state of branch $B(m_k, j_k)$, the corresponding effective work is given by

$$\exp[-\beta\widetilde{\mathcal{W}}^{i \rightarrow k}] = \prod_{m=1}^{m_k-1} \left[\frac{1}{J} \sum_{j=1}^J \exp[-\beta\mathcal{W}(m, j)] \right] \times \exp[-\beta\mathcal{W}(m_k, j_k)]. \quad (20)$$

From a computational point of view, the works $\mathcal{W}(m, j)$ are expressed as a function of the system Hamiltonian (see Eq. (49) of the Appendix). Similarly, the effective works appearing in the Monte Carlo path-average of equation (13) can also be expressed as a function of the Hamiltonian by combining equations (49) and (20) together. We have thus shown how to formally estimate any equilibrium quantity from path-sampling.

4 Application to LJ₃₈

4.1 The LJ₃₈ cluster

We now turn to our application to the 38-atom Lennard-Jones cluster. LJ reduced units of length, energy and mass ($\sigma = 1$, $\varepsilon = 1$, $m = 1$) will be used in the following. LJ₃₈ undergoes a two-stage phase change with increasing temperature [21, 30]. A solid-solid transition between the truncated octahedral funnel and the icosahedral funnel occurs near $T_{ss} \simeq 0.12$, melting follows near $T_{sl} \simeq 0.17$. As in other finite size systems [31], the transitions are not sharp but gradual. The most stable octahedral and icosahedral structures are represented in Figure 1.

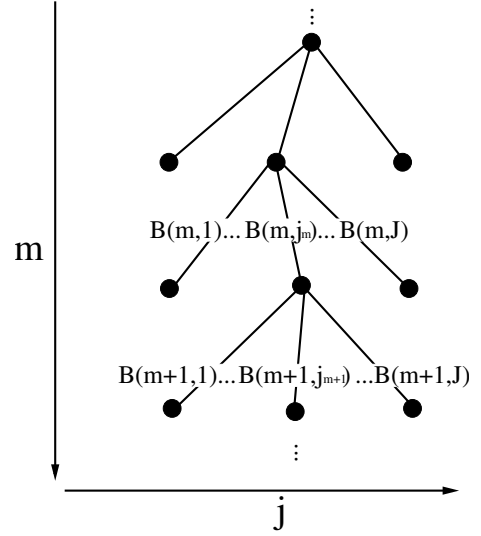


Fig. 2. Schematic representation of a ramified path.

The bond orientational order parameter Q_4 of Steinhardt et al. [19], originally introduced to investigate the glass transition in supercooled liquids, is a convenient reaction coordinate to distinguish between the cubic structure favoured at low temperatures and the icosahedral isomers above T_{ss} . For any given cluster configuration \mathbf{r} , Q_4 is defined as

$$Q_4(\mathbf{r}) = \left(\frac{4\pi}{9} \sum_{m=-4}^4 |\overline{Q}_{4,m}|^2 \right)^{1/2}, \quad (21)$$

where

$$\overline{Q}_{4,m} = \frac{1}{N_b} \sum_{\substack{i < j \\ r_{ij} < r_b}} Y_{4,m}(\theta_{ij}, \phi_{ij}). \quad (22)$$

In the previous equation, r_b is the maximum distance between bonds, N_b the number of such bonds, θ_{ij} and ϕ_{ij} are the polar and azimuthal angles of the vector that points from the cluster center of mass to the center of bond (i, j) . $Y_{4,m}(\theta, \phi)$ is a spherical harmonic.

4.2 Simulation details

A multicanonical-type umbrella sampling simulation is first carried out in the state-ensemble \tilde{Z}_{λ_0} at temperature $T_0 = (k_B\beta\lambda_0)^{-1} = 0.19$, in order to sample the available range of Q_4 and to calculate the free energy profile $\Lambda(Q_4, T_0) = -k_B T_0 \ln p(Q_4, T_0)$, $p(Q_4, T_0)$ being the probability of visiting states with specified values of the order parameter. At this high temperature, a flat-sampling along the Q_4 coordinate of the phase space is more easily achieved. The estimated free energy profile yields the opposite of the auxiliary potential ϕ that will be used subsequently

$$\phi(\mathbf{r}) = -\Lambda[Q_4(\mathbf{r}), T_0]. \quad (23)$$

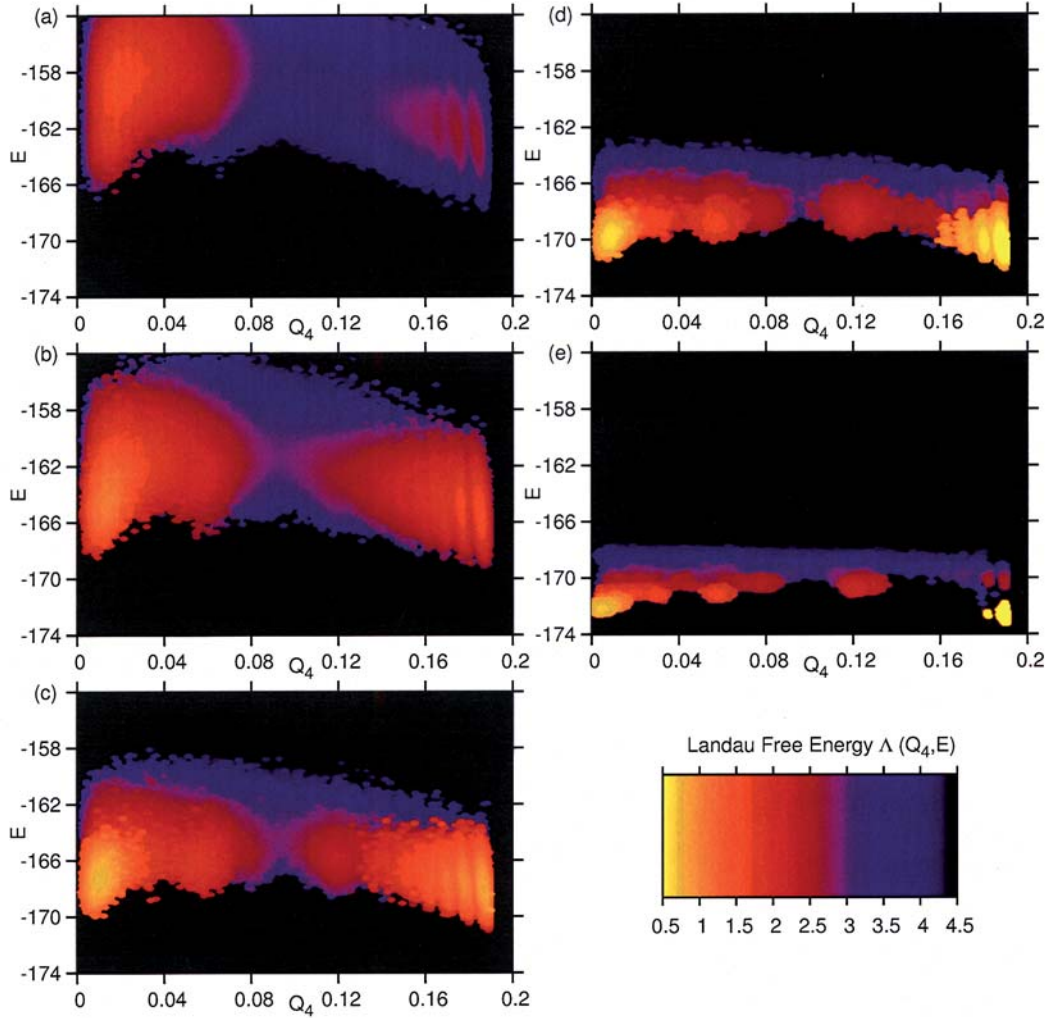


Fig. 3. Contour plot of the Landau free energy $\Lambda(Q_4, E; T)$ for five temperatures (a) $T = 0.19$, (b) $T = 0.147$, (c) $T = 0.105$, (d) $T = 0.062$, (e) $T = 0.021$.

A path-sampling simulation consists in constructing a Markov chain of paths distributed with the $\hat{\mathcal{K}}_{\lambda_0}$ statistics. In other words, the initial states of the paths belong to a Markov chain distributed with the \mathcal{N}_{λ_0} -statistics. The λ -parametrized inverse temperature is chosen to be $\beta_{\lambda_n} = \lambda_n \beta$. The time step τ is adjusted so that the acceptance rate is about 30–60%. The friction parameter of the Langevin-Metropolis dynamics is $\tilde{\gamma} = 2/\tau$ (smaller values were found to be appropriate as well). All reported calculations have been carried out with the following parameters: $M = 100$, $J = 10$ and $N = 2 \times 10^3$ or $N = 2 \times 10^4$. The simulations with $N = 2 \times 10^3$ and $N = 2 \times 10^4$ involve 34 650 and 5818 paths, respectively. These calculations were performed in parallel and took a total of 360 h and 600 h on fifteen 2 GHz Xeon processors, respectively.

4.3 Results

We first computed the Landau free energy as a function of the order parameter Q_4 and internal energy E at constant

temperature T . This physical quantity is defined over the path ensemble as

$$\Lambda(Q_4, E, T) = -k_B T \ln \langle \delta(Q_4(\mathbf{r}_k) - Q_4) \delta(\mathcal{E}(\mathbf{r}_k) - E) |_{\lambda} \rangle, \quad (24)$$

and is estimated using equation (13) where \mathbf{r}_k are the path positions belonging to \mathcal{Z}_{λ} .

Figure 3 displays the contour plots of the Landau free energy for five temperatures ranging from $T = 0.02$ to 0.19. Domains of low free energy, corresponding to high occupation probabilities, evolve significantly as temperature decreases. The icosahedral to octahedral phase change is clearly observed: the most probable structure changes from $Q_4 \sim 0.18$ to $Q_4 \sim 0.02$. As was anticipated, several secondary minima corresponding to liquid-like or defected octahedral structures are visible at sufficiently low temperature, for values of Q_4 ranging from 0.04 to 0.15. The structure corresponding to $Q_4 \sim 0.12$, represented in Figure 4, is a defective truncated octahedron, with missing atoms in the outer shell inducing a stacking fault in the fcc structure. The associated energy and order parameter

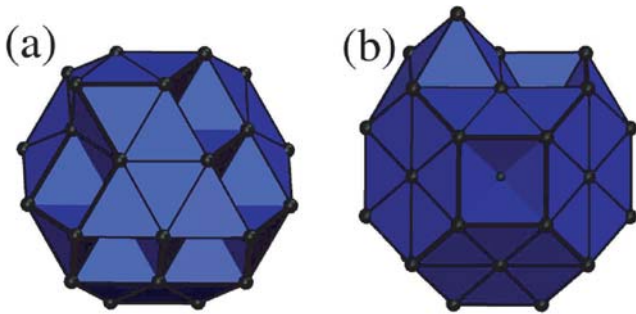


Fig. 4. Structures of the 38-atom defected octahedral cluster. Its minimum energy is -171.8560 and its order parameter is $Q_4 = 0.121$. View (a) emphasizes the stacking fault while view (b) shows the atom that has been expelled from the outer shell.

correspond to one of the energy minima reported by Doye and coworkers [16] who sampled a large set of inherent structures.

Interestingly, the present non-equilibrium approach is not excessively sensitive to the ability of the order parameter to discriminate between all the basins of attraction at low temperature. Some information about the weights of the various inherent structures having similar Q_4 but different energies can be obtained from Figures 3d, 3e in the range $0.04 \leq Q_4 \leq 0.1$. The apparent superposition of the various inherent structures in this figure stems from the multiple peaks of the work-histograms. Figure 5 displays the path distribution in the $(\widetilde{W}^{i \rightarrow k}, Q_4)$ plane at two temperatures. At the lowest temperature, the separate data clouds with similar Q_4 values but different work values correspond to different basins of attraction. Clearly, when the temperature is decreased, the paths are attracted to the various basins and get trapped. The data clouds from Figure 5b having distinct work values, they contribute differently to the canonical average, which yields energy minima patterns that are superimposed in the low temperature contour plots of Figures 3d, 3e.

We now investigate the Landau free energy defined as a function of Q_4 only. In the context of path sampling, $\Lambda(Q_4, T)$ is estimated using

$$\Lambda(Q_4, T) = -k_B T \ln \langle \delta(Q_4(\mathbf{r}_k) - Q_4) |_{\lambda} \rangle, \quad (25)$$

where \mathbf{r}_k are the path positions belonging to \mathcal{Z}_λ . The corresponding free energy landscape, displayed in Figure 6a, clearly shows the secondary free energy basins corresponding to the known energy minima for both the liquid-like structures and the defective octahedron [16]. No low free energy minima seems to have been omitted by our path-sampling approach. The opposite of the derivative of the Landau free energy with respect to temperature defines an entropy σ :

$$\sigma(Q_4, T) = -\partial \Lambda(Q_4, T) / \partial T. \quad (26)$$

σ is not convenient to compute because it is prone to fluctuations at low temperature. Hence, the quantity

$$T\sigma(Q_4, T) = \langle \mathcal{E}(\mathbf{r}_k) \delta(Q_4(\mathbf{r}_k) - Q_4) |_{\lambda} \rangle - \Lambda(Q_4, T)$$

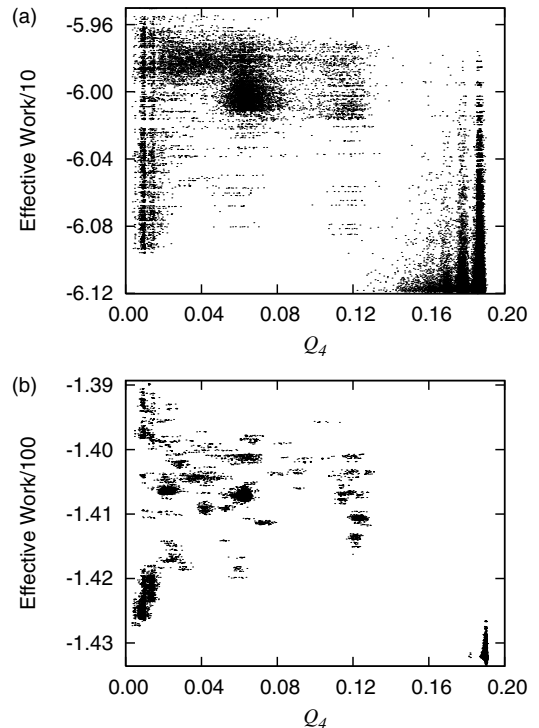


Fig. 5. Effective work distribution as a function of Q_4 and of the effective work at two temperatures: (a) $T = 0.12$; (b) $T = 0.03$, with $N = 2 \times 10^4$ and $M = 10^2$.

has been computed instead; it is represented in Figure 6b. At high temperatures, the high entropy region corresponding to the icosahedral and liquid-like structures is clearly visible.

4.4 Moderate temperature: comparison with other methods

We have compared the present path-sampling method with parallel tempering and Wang-Landau multicanonical sampling. The parallel tempering simulation was carried out with 50 replicas with temperature ranging from 0.01 to 0.35, following a geometric progression. A total of 5×10^9 Monte Carlo cycles have been performed after 10^8 equilibration cycles. These calculations took about 250 h on a serial 2.2 GHz Opteron processor. The Wang-Landau simulations were performed on the joint (E, Q_4) space using the recent annealing scheme explained in reference [22], along with the same technical details. About 150 h were used on a serial 2.2 GHz Opteron processor. The free energy profiles were obtained from suitable weighted-histogram analyses.

Figure 7 shows the free energy profiles computed using the three methods at two distinct temperatures. At the moderate temperature $T = 0.12$ close to the solid-solid transition, the three methods yield results in excellent agreement, which states the correctness of our path-sampling approach. In particular, the nearly equal free energies of the truncated octahedral and icosahedral basins

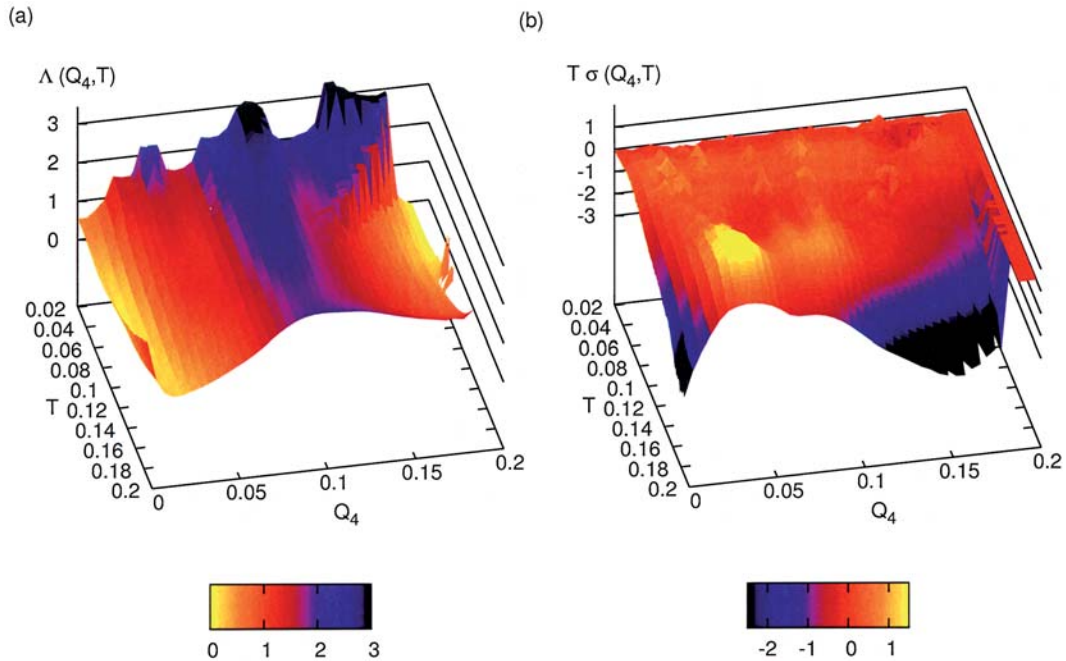


Fig. 6. (a) Landau free energy $\Lambda(Q_4, T)$ and (b) temperature-entropy product $T\sigma(Q_4, T)$ of the LJ₃₈ cluster obtained by path-sampling simulations.

confirm that the transition temperature is close to 0.12 for the three methods.

At the lower temperature $T = 0.05$, only the non-equilibrium approach is able to reveal and separate the contributions from the secondary free energy minima, especially the defective octahedra at $Q_4 = 0.12$. The results obtained with parallel tempering are consistent with a previous study [21], which was also unable to identify this basin of attraction. At such a low temperature, the multi-canonical sampling provided by the Wang-Landau method is likely to fail, and the replicas of parallel tempering only visit the deepest parts of the octahedral and icosahedral funnels. Thus both these methods could be inefficient, despite giving results that agree with each other. To further test the present path-sampling method at low temperatures, we have performed an independent calculation of free energy surfaces using the superposition approximation.

4.5 Comparison with harmonic superposition approximation

Equilibrium properties of clusters, including the partition function itself, can be formally expressed from the contributions of the basins of attraction (or inherent structures) rather than configurations [32,33]. We thus write the partition function of the entire system at the temperature T as the superposition over the set of isomers $\{\alpha\}$:

$$Z(T) = \sum_{\alpha} g_{\alpha} Z_{\alpha}(T), \quad (27)$$

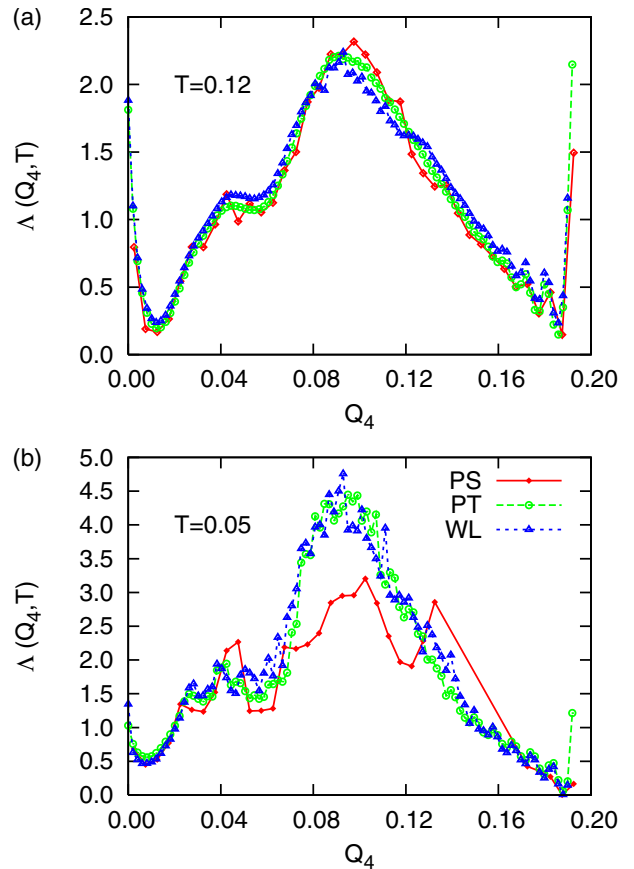


Fig. 7. Landau free energy profiles of LJ₃₈ as a function of Q_4 obtained by path-sampling (PS), parallel tempering (PT) and Wang-Landau (WL) simulations. (a) $T = 0.12$; (b) $T = 0.05$ reduced units.

g_α being a weighting term, which accounts for the number of permutationally equivalent isomers. g_α is related to the order h_α of the point group of isomer α through $g_\alpha = 2N!/h_\alpha$. At low temperature, the harmonic approximation for Z_α is expected to be rather accurate:

$$Z_\alpha(T) = \left(\frac{k_B T}{\hbar \bar{\omega}_\alpha}\right)^\nu \exp\left(-\frac{E_\alpha}{k_B T}\right), \quad (28)$$

with E_α the ground state energy of local minimum α and $\bar{\omega}_\alpha$ the geometrical average of its normal mode frequencies. $\nu = 3N - 6$ is the number of independent degrees of freedom. From equations (27) and (28) the relative probability $p_\alpha = g_\alpha Z_\alpha / Z$ of visiting isomer α is calculated as a function of temperature. Here the harmonic superposition approximation (HSA) is used for comparison with path sampling. The isomers are therefore sorted according to their value of Q_4 , denoted as $Q_4^{(\alpha)}$ for isomer α , and neglecting the variations of $Q_4^{(\alpha)}$ with temperature. Again, this approximation will be satisfied only below T_{ss} . The superposition approximation can provide accurate thermodynamics observables over broad temperature ranges, if anharmonic partition functions are used, and if the minima of the potential energy surface are correctly sampled. For small systems such as LJ₁₃, a nearly complete enumeration of the minima can be performed [37]. However, the number of isomers is likely to grow at least exponentially with the number of degrees of freedom [36], and reweighting schemes [32] are needed for large systems. Anharmonic corrections to the partition functions have been proposed, from either empirical [34] or systematic [35] perturbation expansions. The recent basin-sampling scheme [39] is also a convenient method to sample the relevant isomers, and to incorporate anharmonicities in the partition functions at the same time. Such methods, which aim at characterizing the global thermodynamics of the system over broad temperature ranges, will not be needed here, as we only use the superposition approximation at low temperatures to get an estimate of the relative probabilities of some specific low-energy isomers, particularly the defective truncated octahedra.

Quenches from parallel tempering Monte Carlo simulations provided 6837 different structures, which were gathered into classes depending on their value of Q_4 . The first class $O = \{\alpha | Q_4^\alpha > 0.18\}$ corresponds to the truncated octahedral global minimum, as well as a few defective cubic isomers. The second class, $D = \{\alpha | 0.09 \leq Q_4^\alpha \leq 0.12\}$, contains about half a dozen of defective cubic structures presenting stacking faults. These low energy structures were identified by Doye et al. [16]. The structure of class O with the lowest energy is represented in Figure 4. Finally, the third class I consists of all remaining isomers, including icosahedral and disordered structures.

The probability that the cluster belongs to a particular class X is obtained from the superposition method by the ratio

$$p|_{\text{HSA}}(X, T) = \frac{1}{Z(T)} \sum_{\alpha \in X} g_\alpha Z_\alpha(T), \quad (29)$$

while the Helmholtz and Landau free energies of class X are given by

$$F|_{\text{HSA}}(X, T) = -k_B T \ln \sum_{\alpha \in X} g_\alpha Z_\alpha(T), \quad (30)$$

and

$$\Lambda|_{\text{HSA}}(X, T) = -k_B T \ln p|_{\text{HSA}}(X, T) \quad (31)$$

$$= F|_{\text{HSA}}(X, T) - F_{\text{tot}}(T), \quad (32)$$

respectively, $F_{\text{tot}}(T) = -k_B T \ln Z(T)$ being the total (Helmholtz) free energy of the system at temperature T . Because we will not use any reweighting scheme (thus taking $g_\alpha = 1$ for all α), the free energies calculated this way will not correctly represent the disordered phase, and should not be expected to compare with parallel tempering or Wang-Landau sampling above the melting temperature.

The probability density of class X is obtained from the path-average of equation (13) of the following λ -parametrized function

$$h^X(\mathcal{P}_i^f)|_\lambda = \begin{cases} 1 & \text{if } Q_4(\mathbf{r}_k) \in X \\ 0 & \text{otherwise} \end{cases},$$

where $\mathbf{r}_k \in \mathcal{Z}_\lambda \cap \mathcal{P}_i^f$ and $\lambda = (\beta T)^{-1}$. The reduced Landau free energy of class X is derived from

$$\Lambda(X, T) = -k_B T \ln \langle h^X |_\lambda \rangle.$$

Figure 8 shows the probabilities to find the defective octahedral structure obtained as a function of temperature using either path-sampling or the harmonic superposition approximation. The two methods agree to a very good extent. Some discontinuities are more clearly visible on the Landau free energy; they result from pollutions arising in the octahedral basin. Conversely, the results of parallel tempering and Wang-Landau sampling, also shown on this figure, significantly disagree (even though they agree with each other). This is not surprising, since Figure 7b already showed that defective octahedra were significantly too high in free energy. In other terms, their relative probability is much too small, as precisely seen in Figure 8a.

The free energy profile $F(X; T) = \Lambda(X; T) + F_{\text{tot}}(T)$ is obtained as a function of temperature from the path-average of equation (13) relating the work exponential to the following free energy difference

$$\frac{F_{\text{tot}}(T)}{k_B T} - \frac{F_{\text{tot}}(T_0)}{k_B T_0} = \ln \langle \exp[\beta \widetilde{\mathcal{W}}^{i \rightarrow k}] |_\lambda \rangle \quad (33)$$

$$= -\ln \langle \exp[-\beta \widetilde{\mathcal{W}}^{i \rightarrow k}] |_{\lambda_0} \rangle, \quad (34)$$

where $T_0 = (k_B \beta \lambda_0)^{-1}$, $T = (k_B \beta \lambda)^{-1}$. This average corresponds to a biased implementation of the effective work relation [10].

The free energies obtained from path sampling and from the harmonic superposition approximation are represented in Figure 9. The path-sampling estimation of the

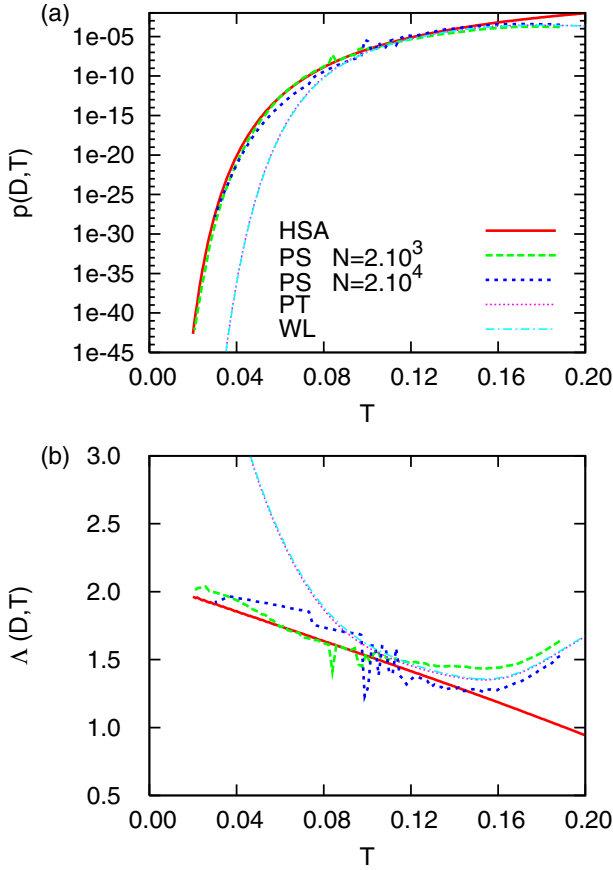


Fig. 8. (a) Occurrence probability and (b) Landau free energy of the defective truncated octahedral cluster as a function of temperature. The results of two path-sampling calculations are shown for two different switching rates. The dotted line corresponds to the harmonic superposition approximation.

solid-solid transition temperature is 0.113 ± 0.05 , in excellent agreement with the estimates from the present parallel tempering and Wang-Landau simulations, as well as previous calculations using these methods [21, 22, 38] (also see Tab. 1). They are slightly below the value given by the harmonic superposition approximation, even though the free energies themselves diverge substantially with increasing temperature. This divergence comes from the way the minima were sampled here (without using a proper reweighting scheme or basin-sampling), more than the neglect of anharmonic contributions to the free energies. It is likely that these contributions are quantitatively similar for the icosahedral and octahedral structures, otherwise the Landau free energies of these two structures would disagree with respect to the ones given by the harmonic approximation. Finally, and while the bidimensional Wang-Landau calculations performed here agree with path-sampling, we note that the more conventional one-dimensional Wang-Landau sampling based on energy histograms only yields an incorrect estimate of the transition temperature [39].

We also find from Table 1 that the transition temperature T_{ss} estimated from path-sampling is sensitive to the length of the path, via the N parameter. This makes it

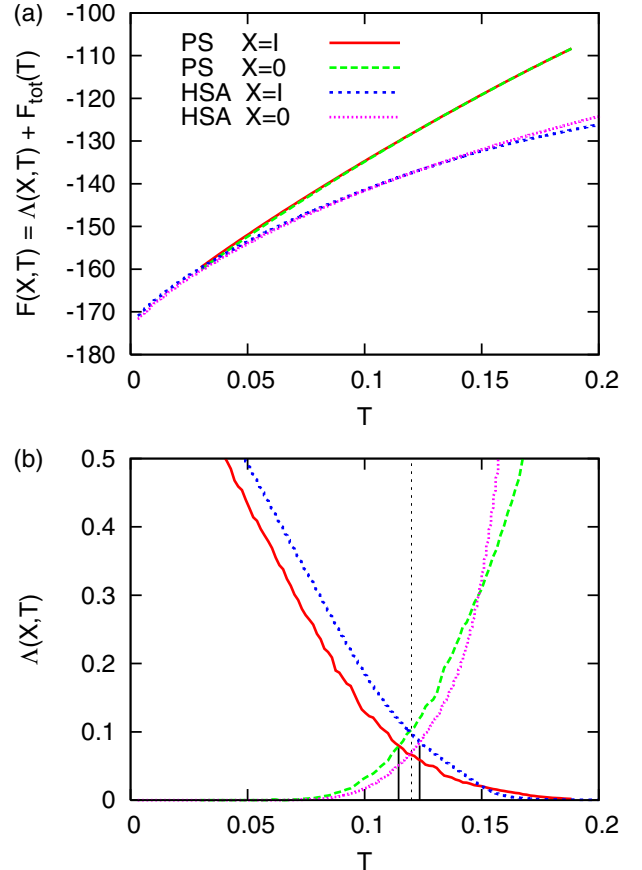


Fig. 9. (a) Helmholtz free energies and (b) Landau free energies of the truncated octahedral (O) and icosahedral (I) basins, as a function of temperature. Symbols and lines represent the path-sampling (PS) estimates and the harmonic superposition approximation (HSA), respectively. Small vertical bars are drawn to indicate the PS and HSA solid-solid transition temperatures. The dashed vertical line indicates the transition temperature obtained from parallel tempering and Wang-Landau sampling.

necessary to carry out simulations with increasing N until the estimated T_{ss} reaches a plateau.

From the above study, the path-sampling approach can be confidently used to probe the low-temperature properties of the energy landscape. We believe that the disagreement in the Landau free energy profiles obtained using either path-sampling or state-sampling methods such as parallel tempering or the Wang-Landau algorithm reflects some intrinsic difficulties met by equilibrium methods.

4.6 Discussion

The present investigation shows that a non-equilibrium approach allows the contribution of all important inherent structures to be incorporated in canonical averages, even at very low temperatures. In the path-sampling approach, the free energy provides information about the probabilities to find any particular structure, whereas in state-sampling methods the probabilities computed beforehand

Table 1. Temperature of the structural transition between the octahedral and icosahedral structures estimated using different methods. Path-sampling data are obtained with a comparable numerical cost.

Method	T_{ss}
Harmonic Superposition Approximation	0.12
Anharmonic Superposition Approximation	0.11 [16]
Parallel Tempering	0.12 [21]
	0.11 [38]
Wang-Landau sampling with	
E -histograms	0.09 [39]
(E, Q_4) -histograms	0.12 [22]
Path-sampling	
$N = 2 \times 10^2$	0.09 ± 0.01
$N = 2 \times 10^3$	0.104 ± 0.005
$N = 2 \times 10^4$	0.113 ± 0.005

are transformed into free energies. From a quantitative point of view, the transition temperature obtained from equating the free energies of the two important funnels also agree with state-sampling methods.

The main limitation of the present path-sampling approach is the lack of built-in tool for estimating the convergence of the simulations. A possible way to solve this problem would be to analyse on the fly the overlaps between the reference and target path-work histogram [24]. This can be achieved by generating trajectories backward in time using the conditional probabilities of the $\hat{\mathcal{Z}}_{\lambda_1}$ target ensemble and accepting them using a Metropolis algorithm in which the a priori probability to generate the trial paths coincides with the conditional path probabilities. This procedure corresponds in fact to the shooting algorithm developed initially for sampling transition pathways [11,40], recently extended to non-equilibrium paths [15,24,41] in generalized ensembles. Markov chains of paths distributed with respect to any targeted ensemble can thus be obtained even if the trial paths are generated with respect to a different reference ensemble.

An important point is that an optimal switching rate must be chosen in order to maintain the states along the trajectories in an appropriate local equilibrium. If the switching rate is too high, entropy is produced by dissipating work, which leads to broad work distributions and insufficient overlap between the reference and the target ensembles. The Monte Carlo averages become then dominated by a few rare paths and numerical convergence is poor. This was evidenced here on the inaccurate estimates of the transition temperatures between the truncated octahedral and icosahedral funnels. Conversely, in the limit of very small switching processes, the states along the trajectories are distributed in a more global equilibrium. Therefore, excursions to secondary basins of attraction occur with a lower probability, they are sampled only occasionally, and numerical efficiency also decreases. Finding an appropriate balance between these two undesirable situations should thus be crucial for successful applications of the path-sampling method.

We also mention that the typical computer time needed by path-sampling simulations to obtain appar-

ently converged results exceeds the times needed by either parallel tempering or Wang-Landau sampling, by about one order of magnitude. Even though path-sampling takes considerable time, it found the defective octahedron very quickly. The extra computer time is required to reduce statistical fluctuations. To speed up path-sampling calculations in future works, especially when constructing free energy landscapes, it might be advantageous to extract more information from individual paths while still using very slow switching rates.

5 Concluding remarks

In the present study, we have presented a biased path-sampling technique that allows the energy and free energy landscapes of complex many-body system to be accurately computed. The statistical biases are based on several techniques commonly used in conventional state sampling. Firstly, a multicanonical-type umbrella potential is included when sampling the initial states of the paths and maintained when propagating the paths, allowing a much more efficient exploration of the various competing basins of attraction on the potential energy surface. Secondly, the ensemble-average is carried out with respect to a reference ensemble differing from the targeted ensemble. This is accounted in the ensemble average by weighting the paths using a correcting factor corresponding to the exponential of an effective work. Thirdly, paths are generated more efficiently using a configurational-bias scheme, hence the sampling procedure incorporates a Rosenbluth factor.

Owing to the non-equilibrium character of the path-sampling averages, information from different basins of attraction can be gathered provided that a sufficient number of trajectories are accumulated. This strategy somewhat contrasts with the parallel tempering where the multiple temperatures are introduced to avoid trapping in the secondary energy minima.

The path-sampling scheme was successfully applied to the well-documented LJ₃₈ atomic cluster system. For slow switching simulations, the estimated solid-solid transition temperature between the truncated octahedral and icosahedral funnels was found to be in agreement with the values given by other simulation methods, including parallel tempering and Wang-Landau Monte Carlo methods. The Landau free energy was calculated as a function of the bond orientational order parameter Q_4 at several temperatures. The variations of this quantity were seen to be accurately reproduced, not only at moderate or high temperatures where the aforementioned state-sampling methods are efficient, but also at low temperatures, by comparing to the predictions of an independent harmonic superposition calculation. In particular, all important secondary energy minima were found, and correctly weighted, by the path-sampling approach. In contrast, both parallel tempering and two-dimensional Wang-Landau sampling failed in sampling the defective truncated octahedron with a quantitative probability. For the presently investigated LJ₃₈ system, the path-sampling method provides access

to more details of the free energy landscape than conventional state-sampling techniques. To our knowledge, this is the first time that a non-equilibrium approach is found to be superior to equilibrium methods.

Future works should probably compare path-sampling to the improvements and extensions of parallel tempering that have been recently proposed [38,42–45], or with the basin-sampling scheme [39]. In the latter case, one would probably also need to estimate how the order parameter varies with temperature for the isomers sampled.

The simultaneous use of several generalized ensemble strategies, by combining for instance multicanonical or umbrella sampling approaches with parallel tempering, seems promising. However, and in general, biasing along an appropriate order parameter by umbrella or multicanonical sampling seems a key to the success of these methods, including path-sampling, even though state-sampling methods are more sensitive to the choice of the order parameter. Therefore, the present path-sampling approach provides a broader framework to calculate free energies for complex systems with rugged energy landscapes, down to low temperatures where current approaches may not be so accurate.

Fruitful discussions with N. Mousseau, D. Frenkel, M. Parrinello, C. Dellago, and P. Bolhuis are gratefully acknowledged.

Appendix: Langevin-Metropolis algorithm for propagating the paths

A hybrid Langevin-Metropolis algorithm is implemented to generate the initial states of the paths at $\lambda = \lambda_0$ and to propagate the paths with λ varying from λ_0 to λ_1 .

Solving the Langevin dynamics requires a continuous Hamiltonian gradient. Here, the parametrized Hamiltonian \mathcal{H}_λ , is not continuously derivable with respect to the particle positions because it contains the auxiliary umbrella potential, ϕ , which depends on the discontinuous order parameter Q_4 . Consequently, the interparticle force

$$\mathbf{f}_n^\lambda = \nabla_{\mathbf{r}_n} [\phi(\mathbf{r}_n) - \mathcal{H}_\lambda(\mathbf{r}_n, \mathbf{p}_n)] \quad (35)$$

$$= -\lambda_n \nabla_{\mathbf{r}_n} \mathcal{E}(\mathbf{r}_n) = \lambda_n \mathbf{f}_n \quad (36)$$

are used to propagate trial Langevin dynamics ($\lambda_n = \beta\lambda_n/\beta$). The Metropolis algorithm is subsequently implemented to accept or reject these trial moves with respect to the targeted canonical distribution of the \mathcal{H}_λ -system.

Here, we describe this hybrid algorithm and derive the ratio of the forward and backward probability fluxes, which are key ingredients of path-sampling. From state $\mathcal{S}_n = (\mathbf{r}_n, \mathbf{p}_n)$ the trial state $\mathcal{S}'_{n+1} = (\mathbf{r}'_{n+1}, \mathbf{p}'_{n+1})$ is gen-

erated using the following updating scheme

$$\mathbf{p}_{n+\frac{1}{4}} = \mathbf{p}_n + \ell_{n+\frac{1}{4}} \frac{\tau}{2} \quad (37)$$

$$\mathbf{p}_{n+\frac{1}{2}} = \mathbf{p}_{n+\frac{1}{4}} + \lambda_n \mathbf{f}_n \frac{\tau}{2} \quad (38)$$

$$\mathbf{r}'_{n+1} = \mathbf{r}_n + \mathbf{p}_{n+\frac{1}{2}} \frac{\tau}{m} \quad (39)$$

$$\mathbf{p}_{n+\frac{3}{4}} = \mathbf{p}_{n+\frac{1}{2}} + \lambda_n \mathbf{f}_{n+1} \frac{\tau}{2} \quad (40)$$

$$\mathbf{p}'_{n+1} = \mathbf{p}_{n+\frac{3}{4}} + \ell_{n+\frac{3}{4}} \frac{\tau}{2} \quad (41)$$

where τ is the time step, \mathbf{f}_n^λ is the energy gradient and $\ell_{n+\frac{2\pm 1}{4}}$ are the discretized stochastic forces:

$$\ell_{n+\frac{1}{4}} = -\mathbf{p}_n \tilde{\gamma} \frac{\tau}{2} + \mathbf{b}_{n+\frac{1}{4}}^+ \sqrt{\frac{m}{\beta} \tilde{\gamma} \tau \left(1 - \tilde{\gamma} \frac{\tau}{4}\right)} \quad (42)$$

$$\ell_{n+\frac{3}{4}} = \mathbf{p}_{n+\frac{1}{4}} \tilde{\gamma} \frac{\tau}{2} + \mathbf{b}_{n+\frac{3}{4}}^- \sqrt{\frac{m}{\beta} \tilde{\gamma} \tau \left(1 - \tilde{\gamma} \frac{\tau}{4}\right)} \quad (43)$$

where $\mathbf{b}_{n+\frac{1}{4}}^+$ and $\mathbf{b}_{n+\frac{3}{4}}^-$ are the forward and backward normal noises of zero mean and unit variance, respectively. $\tilde{\gamma}$ is the effective friction. The updating scheme corresponds to the leap-frog scheme of reference [15] and is obtained here from the Trotter factorization of the evolution operator [24]. More precisely, the updates of equations (37) and (41) integrate the stochastic part of the Langevin equation, $\dot{\mathbf{p}} = -\gamma \mathbf{p} + \mathbf{b} \sqrt{2m\gamma/\beta}$, over $\tau/2$ where the friction is

$$\gamma = -\frac{2}{\tau} \ln \left[1 - \frac{\tilde{\gamma} \tau}{2} \right].$$

The backward to forward probability ratio to generate $\ell_{n+\frac{1}{4}}$ writes

$$\begin{aligned} \frac{P^-(\ell_{n+\frac{1}{4}})}{P^+(\ell_{n+\frac{1}{4}})} &= \exp \left[-\frac{1}{2} \left(|\mathbf{b}_{n+\frac{1}{4}}^-|^2 - |\mathbf{b}_{n+\frac{1}{4}}^+|^2 \right) \right] \\ &= \exp \left[-\frac{\beta}{2m} \left(\mathbf{p}_n^2 - \mathbf{p}_{n+\frac{1}{4}}^2 \right) \right]. \end{aligned} \quad (44)$$

This was derived by expressing the normal probabilities associated to $\mathbf{b}_{n-\frac{1}{4}}^\pm$ as a function of \mathbf{p}_n and $\mathbf{p}_{n+\frac{1}{4}}$ by means of equation (43). A similar equality holds for the probability ratio involving $\ell_{n+\frac{3}{4}}$:

$$\frac{P^-(\ell_{n+\frac{3}{4}})}{P^+(\ell_{n+\frac{3}{4}})} = \exp \left[-\frac{\beta}{2m} \left(\mathbf{p}_{n+\frac{3}{4}}^2 - \mathbf{p}_{n+1}^2 \right) \right]. \quad (45)$$

The ratio of the backward to forward trial probability flux is therefore

$$\rho_{n+\frac{1}{2}}^+ = \frac{\exp[-\beta \mathcal{H}^{\lambda_n}(\mathcal{S} + \phi'_{n+1})'_{n+1}] P^-(\ell_{n+\frac{1}{4}}) P^-(\ell_{n+\frac{3}{4}})}{\exp[-\beta \mathcal{H}^{\lambda_n}(\mathcal{S}_n) + \phi_n] P^+(\ell_{n+\frac{1}{4}}) P^+(\ell_{n+\frac{3}{4}})},$$

where $\phi'_{n+1} = \phi(\mathcal{S}'_{n+1})$, $\phi_n = \phi(\mathcal{S}_n)$, $\mathcal{E}'_{n+1} = \mathcal{E}(\mathbf{r}'_{n+1})$ and $\mathcal{E}_n = \mathcal{E}(\mathbf{r}_n)$. This equality can be simplified by using

equations (44) and (45) as follows

$$\rho_{n+\frac{1}{2}}^+ = \exp \left[-\beta \lambda_n (\mathcal{E}'_{n+1} - \mathcal{E}_n) - \frac{\beta}{2m} (\mathbf{p}_{n+\frac{3}{4}}^2 - \mathbf{p}_{n+\frac{1}{4}}^2) \right] \times \exp [\phi'_{n+1} - \phi_n]. \quad (46)$$

This trial probability ratio is incorporated into a Metropolis Monte Carlo algorithm. The probability to accept the move is

$$\text{acc}(n \rightarrow n+1) = \min \left(1, \rho_{n+\frac{1}{2}}^+ \right). \quad (47)$$

If the move is accepted, then $\mathcal{S}_{n+1} = (\mathbf{r}'_{n+1}, \mathbf{p}'_{n+1})$, otherwise, the trial state is rejected and \mathcal{S}_{n+1} is set to $(\mathbf{r}_n, -\mathbf{p}_n)$. Recalling that the backward trajectory is constructed using the reversed momenta of the forward trajectory, a rejection event occurs with a probability that is identical for both the forward and backward directions:

$$\begin{aligned} \text{acc}(n \rightarrow n+1) &= 1 - \rho_{n+\frac{1}{2}}^+ \\ &= \text{acc}(n+1 \rightarrow n). \end{aligned} \quad (48)$$

Similarly, the a priori probabilities to generate the rejected trial states are terms appearing identically both in the forward and backward probability fluxes, which leads to their cancellation [41]. Hence, at constant λ_n , the present procedure always guarantees a strict equality between the forward and backward probability fluxes [41]. However, since λ_n evolves during the Langevin-Metropolis dynamics, the ratio of the backward to forward probability flux is no more unity.

A branch $B(m, j)$ of the ramified path is constructed by iterating N times the Langevin-Metropolis algorithm with increasing the coupling parameter from $\lambda_{N(m-1)}$ to λ_{Nm} . It results that a certain amount of work is introduced from the outside world into the system constituted by the particles and the thermostat. This work can be expressed as follows

$$\begin{aligned} \mathcal{W}(m, j) &= \sum_{n=N(m-1)}^{Nm-1} [\mathcal{H}^{\lambda_{n+1}}(\mathbf{r}_n, \mathbf{p}_n) - \mathcal{H}^{\lambda_n}(\mathbf{r}_n, \mathbf{p}_n)] \\ &= \sum_{n=N(m-1)}^{Nm-1} (\lambda_{n+1} - \lambda_n) \mathcal{E}_n \end{aligned} \quad (49)$$

and exactly determines the probability flux ratio

$$\frac{\mathcal{N}_{\lambda_{Nm}}(\mathcal{S}_{Nm}) P_{gen}^-(m, j)}{\mathcal{N}_{\lambda_{N(m-1)}}(\mathcal{S}_{N(m-1)}) P_{gen}^+(m, j)} = \exp[-\beta \mathcal{W}(m, j)] \quad (50)$$

where the probability $P_{gen}^\pm(m, j)$ to generate the branch $B(m, j)$ forward or backward in time is the product of probabilities to generate the trial states and to accept or to reject them.

Finally, notice that the acceptance rate is determined by the variations of the auxiliary field ϕ and the discretization error. From equations (38), (39) and (40), one has

$$\mathbf{p}_{n+\frac{3}{4}} - \mathbf{p}_{n+\frac{1}{4}} = \lambda_n (\mathbf{f}'_{n+1} + \mathbf{f}_n) \frac{\tau}{2} \quad (51)$$

$$\mathbf{p}_{n+\frac{3}{4}} + \mathbf{p}_{n+\frac{1}{4}} = (\mathbf{r}'_{n+1} - \mathbf{r}_n) \frac{m}{2\tau}, \quad (52)$$

which yields

$$\begin{aligned} \frac{1}{2m} (\mathbf{p}_{n+\frac{3}{4}}^2 - \mathbf{p}_{n+\frac{1}{4}}^2) &= \lambda_n (\mathbf{f}'_{n+1} + \mathbf{f}_n) \times (\mathbf{r}'_{n+1} - \mathbf{r}_n) / 2 \\ &= -\lambda_n (\mathcal{E}'_{n+1} - \mathcal{E}_n) + \mathcal{O}(\tau^4). \end{aligned} \quad (53)$$

Hence, the ratio of the backward to forward trial probability flux is

$$\rho_{n+\frac{1}{2}}^+ = \exp [\mathcal{O}(\tau^4) + \phi'_{n+1} - \phi_n]. \quad (54)$$

Because the $\mathcal{O}(\tau^4)$ term slowly increases with the time step τ , and also because the umbrella potential slowly evolves with the cluster structure, an acceptance rate in the 30–60% range can be obtained, even for quite long time steps.

References

1. G.M. Torrie, J.P. Valleau, *J. Comput. Phys.* **23**, 187 (1977)
2. B.A. Berg, T. Neuhaus, *Phys. Lett. B* **267**, 249 (1991)
3. B.A. Berg, T. Neuhaus, *Phys. Rev. Lett.* **68**, 9 (1992)
4. E. Marinari, G. Parisi, *Europhys. Lett.* **19**, 451 (1992)
5. J. VandeVondele, U. Röthlisberger, *J. Chem. Phys.* **113**, 4863 (2000)
6. F. Wang, D.P. Landau, *Phys. Rev. Lett.* **86**, 2050 (2001)
7. F. Calvo, *Molec. Phys.* **100**, 3421 (2003)
8. E.A. Carter, G. Ciccotti, J.T. Hynes, R. Kapral, *Chem. Phys. Lett.* **156**, 472 (1989)
9. W. Watanabe, W.P. Reinhardt, *Phys. Rev. Lett.* **65**, 3301 (1990)
10. C. Jarzynski, *Phys. Rev. Lett.* **78**, 2690 (1997)
11. C. Dellago, P.G. Bolhuis, F.S. Csajka, D. Chandler, *J. Chem. Phys.* **108**, 1964 (1998)
12. D.J. Wales, *Molec. Phys.* **100**, 3285 (2002)
13. D.M. Ceperley, *Rev. Mod. Phys.* **67**, 279 (1995)
14. P.A. Frantsuzov, V.A. Mandelshtam, *J. Chem. Phys.* **121**, 9247 (2004)
15. M. Athènes, *Eur. Phys. J. B* **38**, 651 (2004)
16. J.P.K. Doye, M.A. Miller, D.J. Wales, *J. Chem. Phys.* **110**, 6896 (1999)
17. M.A. Miller, J.P.K. Doye, D.J. Wales, *Phys. Rev. E* **60**, 3701 (1999)
18. D.J. Wales, *Molec. Phys.* **102**, 891 (2004)
19. P.J. Steinhardt, D.R. Nelson, M. Ronchetti, *Phys. Rev. B* **28**, 784 (1983)
20. G.J. Geyer, in *Computing Science and Statistics: Proceedings of the 23rd Symposium on the Interface*, edited by E.K. Keramidas (Interface Foundation, Fairfax Station, 1991), p. 156
21. J.P. Neirotti, F. Calvo, D.L. Freeman, J.D. Doll, *J. Chem. Phys.* **112**, 10340 (2000); F. Calvo, J.P. Neirotti, D.L. Freeman, J.D. Doll, *J. Chem. Phys.* **112**, 10350 (2000)
22. P. Poulain, F. Calvo, R. Antoine, M. Broyer, Ph. Dugourd, *Phys. Rev. E* **73**, 056704 (2006)
23. D. Wu, D.A. Kofke, *J. Chem. Phys.* **122**, 204104 (2005)
24. G. Adjanor, M. Athènes, *J. Chem. Phys.* **121**, 234104 (2005)
25. D. Frenkel, B. Smit, *Understanding molecular simulation*, 2nd edn. (Academic Press, San Diego, 2003)
26. J.A. Siepmann, D. Frenkel, *Molec. Phys.* **75**, 59 (1992)

27. G.N. Bochkov, Yu.E. Kuzovlev, *J. Exp. Theor. Phys.* **45**, 125 (1978)
28. G.N. Bochkov, Yu.E. Kuzovlev, *Physica A* **106**, 481 (1981)
29. G.E. Crooks, *Phys. Rev. E* **61**, 2361 (2000)
30. J.P.K. Doye, D.J. Wales, *Phys. Rev. Lett.* **80**, 1357 (1998); J.P.K. Doye, D.J. Wales, M.A. Miller, *J. Chem. Phys.* **109**, 8143 (1998)
31. J. Jortner, *Z. Phys. D: At. Mol. Clusters* **24**, 247 (1992)
32. D.J. Wales, *Molec. Phys.* **78**, 151 (1993)
33. F. Calvo, J.P.K. Doye, D.J. Wales, *Chem. Phys. Lett.* **366**, 176 (2002)
34. J.P.K. Doye, D.J. Wales, *J. Chem. Phys.* **102**, 9659 (1995)
35. F. Calvo, J.P.K. Doye, D.J. Wales, *J. Chem. Phys.* **115**, 9627 (2001)
36. F.H. Stillinger, *Phys. Rev. E* **59**, 48 (1999)
37. D.J. Wales, *Energy Landscapes* (Cambridge University Press, Cambridge, 2003)
38. F. Calvo, *J. Chem. Phys.* **123**, 124106 (2005)
39. T.V. Bogdan, D.J. Wales, F. Calvo, *J. Chem. Phys.* **124**, 044102 (2006)
40. C. Dellago, P.G. Bolhuis, P. Geissler, *Adv. Chem. Phys.* **123**, 1 (2002)
41. M. Athènes, *Phys. Rev. E* **64**, 046705 (2002)
42. F. Calvo, J.P.K. Doye, *Phys. Rev. E* **63**, 010902 (2000)
43. Y. Sugita, A. Kitao, Y. Okamoto, *J. Chem. Phys.* **113**, 6042 (2000)
44. Y. Sugita, Y. Okamoto, *Chem. Phys. Lett.* **329**, 261 (2000)
45. R. Faller, Q. Yan, J.J. de Pablo, *J. Chem. Phys.* **116**, 5419 (2002)